

Calibration of the Planetary Fourier Spectrometer short wavelength channel

M. Giuranna^{a,*}, V. Formisano^a, D. Biondi^a, A. Ekonomov^b, S. Fonti^c, D. Grassi^a,
H. Hirsch^d, I. Khatuntsev^b, N. Ignatiev^{b,a}, M. Michalska^e, A. Mattana^a, A. Maturilli^a,
B.E. Moshkin^b, E. Mencarelli^a, F. Nespoli^a, R. Orfei^a, P. Orleanski^e, G. Piccioni^f,
M. Rataj^e, B. Saggin^g, L. Zasova^{b,a}

^a*Istituto di Fisica dello Spazio Interplanetario CNR (IFSI), Via del Fosso del Cavaliere 100, 00133 Roma, Italy*

^b*Space Research Institute of Russian Academy of Sciences (IKI), Profsojuznaja 84/32, 117810 Moscow, Russia*

^c*Dipartimento di Fisica, Università degli Studi di Lecce, Via Arnesano, 73100 Lecce, Italy*

^d*Deutsche Forschungsanstalt für Luft und Raumfahrt (DLR), Institut für Planetenerforschung, Rudower Chaussee 5, 12489 Berlin Adlershof, Germany*

^e*Space Research Center of Polish Academy of Sciences (SRC PAS), Bartycka 18A, 00716 Warsaw, Poland*

^f*Istituto Astrofisica Spaziale CNR (IAS), 00185 Roma, Italy*

^g*Università di Padova, Dipartimento Ingegneria Meccanica (DIUNP), Via Venezia 1, 35131 Padova, Italy*

Received 3 June 2004; received in revised form 29 October 2004; accepted 13 December 2004

Available online 13 June 2005

Abstract

The Planetary Fourier Spectrometer (PFS) experiment on board the Mars Express mission has two channels covering the 1.2–5.5 μm short wavelength channel (SWC) and the 5.5–45 μm (LWC). The SWC measures part of the thermal emission spectrum and the solar reflected spectrum of Mars between 1700 and 8200 cm^{-1} with a spectral resolution of 1.3 cm^{-1} , in absence of apodisation. We present here the calibration of this channel and its performance. The instrument calibration has been performed on ground, before launch, in space during near earth verification (NEV) measurements, and at Mars. Special attention has been given to the problem of microvibrations on board the spacecraft.

In order to obtain correct results, the source–instrument–detector interaction for the thermal part is studied very accurately. The instrument shows a nonlinear behaviour with source intensity. The SNR increases with amplification, hence high gain factors are usually used. The detector is, in space, cooled by a passive radiator, and works around 210–215 K. The calibration source (an internal lamp) shows variations during a pericentre pass and therefore impose a complex procedure for the SW channel calibration. Mechanical microvibrations strongly affect part of the spectrum. We discuss the validity of the present calibration, and indicate possible future developments. Samples of the calibrated data are given to show the performance of the experiment and its scientific potentialities.

© 2005 Elsevier Ltd. All rights reserved.

1. Introduction

The Planetary Fourier Spectrometer (PFS) has been described in Paper I (Formisano and the PFS Team, 2005a). The long wavelength channel calibration has been given in Paper II (Giuranna et al., 2005). Here we discuss the short wavelength channel calibration

of PFS. The SW channel was designed to record the Martian infrared spectrum between 1.2 and 5.0 μm (2000–8200 cm^{-1}), a posteriori we found that it is actually able to cover the Martian spectrum down to 1700 cm^{-1} . This is a favourable result because the wavenumber range of the LW channel 1700–2000 cm^{-1} is essentially destroyed by the microvibrations present on the Mars Express spacecraft. The SW channel has a spectral resolution of $\sim 1.3 \text{ cm}^{-1}$ (samples every 1.02 cm^{-1}).

*Corresponding author.

E-mail address: marco.giuranna@ifsi.rm.cnr.it (M. Giuranna).

The purpose of this paper is to present the radiometric and spectral performances of the short wavelength channel (SWC) resulting from the ground calibrations first and in space later and presently at Mars.

The SWC detector is a photoconductor device working at cooled temperature $T_o = 200\text{--}220\text{ K}$. AS a consequence of having the same channel/detector for a wide wavenumber range, the SWC aims to measure two different regimes: the thermal radiation and the solar reflected radiation. This implies two different detector–instrument–source behaviours: in the thermal regime we have an interaction similar to the one studied for the LW channel, while in the solar radiation range this interaction is negligible: the solar radiation in the $1.2\text{--}4\ \mu\text{m}$, if expressed in terms of thermal brightness, would give temperatures very high and certainly much higher than detector temperature ($T_d = 210\text{ K}$) and instrument temperature ($T_i = 283\text{ K}$); in the thermal radiation range PFS SW channel is sensitive to the temperature difference between the emitting source (T_s) and the detector temperature; the amplitude of the measured signal therefore depends upon $\Delta T = |T_o - T_s|$. The thermal conditions of the instrument are therefore very important: in the laboratory we were not able to stabilise the detector temperature at $200\text{--}220\text{ K}$ as required, while in space, although not stable, these temperatures are well reached. We show in Fig. 1 the SW channel detector temperature during one typical pericentre pass. The temperature was around 212 K when observing Mars, but was varying during the calibration activity (first and last 30 measurements). It is important to add in these introductory notes that PFS SW channel has a clear detectable signal not only when observing the internal Black Body source, but also when observing Deep Space. In this sense it is acting like the LW channel, and we refer to Paper II for all general comments.

We shall present here first the results of the Laboratory calibrations (nonlinearity, field of view (FOV), gain factors, Internal Calibration Lamp, Thermal behaviour, etc.), then the Near Earth Verification calibrations (Internal Calibration Lamp partial failure, contamination of the pointing mirror, spacecraft microvibrations, etc.), and finally the calibrations at Mars. We shall conclude with some calibrated spectra to show the performance and capability of PFS.

2. Laboratory measurements

2.1. Calibration sources

The PFS SWC has been calibrated in laboratory mainly by means of four calibration sources. Two were the same as for the thermal part (LW channel):

- The “IFSI” blackbody (MIKRON M345 \times 4 UDC), with a manufacturer certified emissivity of 0.970 ± 0.005 in the ranges $8\text{--}15$ and $3\text{--}5\ \mu\text{m}$.
- The “IKI” blackbody, developed in Russia, but available in IFSI with an emissivity of 0.9 ± 0.1 .
- The “Integrating sphere”, Optronic Lab. Inc. OL 455 12 2. This source provides the radiance spectrum from 4000 to 8200 cm^{-1} given by the maker when the current is fixed to a value (5440 mA). The output is then fixed to 5403 foot-Lamberts (fL) and can be linearly varied by opening or closing a slit aperture by means of micrometer device.
- The “Mercury Lamp”: Oriel 6035. Very stable against temperature variations. It provides a number of Hg lines, but the strongest is at 6537.74 cm^{-1} . The width of the line is declared “negligible” by the maker, with no precise value.

The Internal Black Body (emissivity 0.99, measured temperature accurate to 0.01 K) located in the Scanner Unit, and the Internal Calibration Lamp were also used, the last one being a lamp source focused on the detector.

In the Lab we studied the Linearity of the instrument, the variation with the gain factors, the temperature dependence of the responsivity and noise equivalent radiance (NER), the temperature dependence of the laser diode wavelength used to sample the interferogram at constant optical path differences, the monochromatic transfer function, the FOV and stray light. In all, the Laboratory measurements performed in open atmosphere, the thermal control was not operating and the devices were at room temperature.

2.2. Linearity

The PFS in the SW channel is a nonlinear instrument for intense sources. We have indeed found that the peak of symetrised interferogram (see Appendix A), which is proportional to the total energy content of the spectrum, increases linearly only for small intensity values of the source (up to 280 fL), above which the departure from linearity became bigger and bigger for increasing source intensities.

A procedure for linearising the interferograms was implemented and tested. The fits to the two curves given in Fig. 2 are

$$y = ax^2 + bx + c, \quad (1)$$

$$y = a_1x + b_1, \quad (2)$$

where $a = -0.000115313$, $b = 1.96436$, $c = 706.254$, $a_1 = 4.56359$, $b_1 = 0.0$; x and y are, respectively, the source intensity (in fL) and the amplitude of the peak of the interferogram (Digital Numbers “DN”).

The correction of the interferogram is needed for all the values that with gain 1 are equal or above 1250 DN .

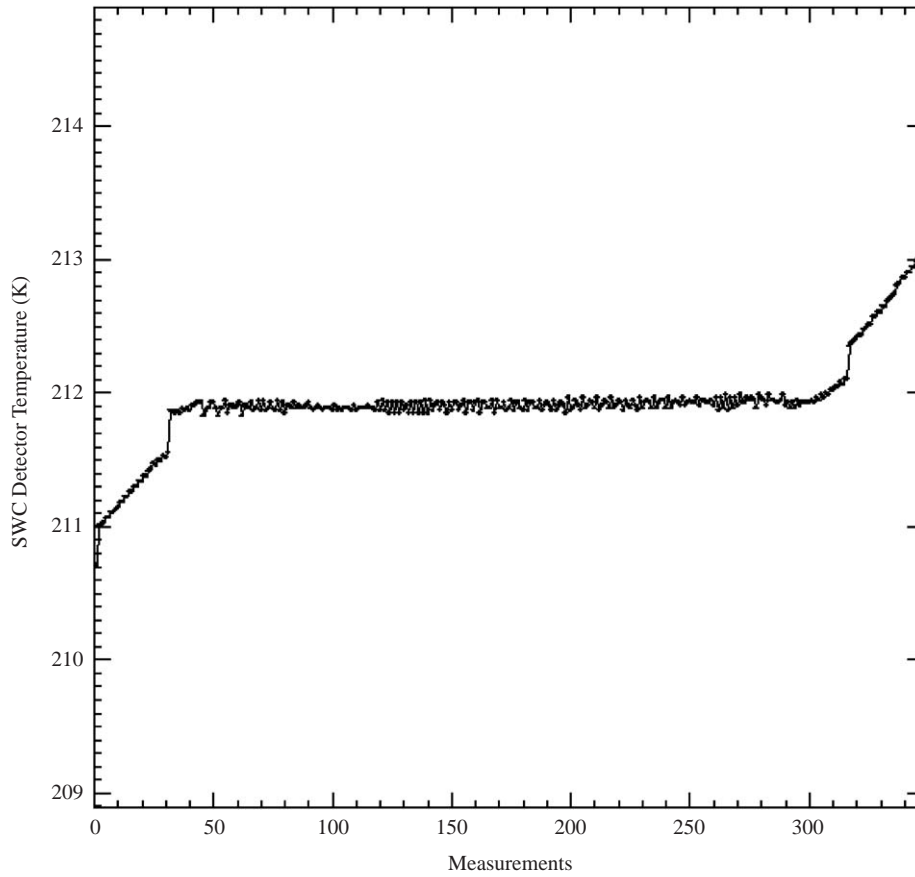


Fig. 1. Short wavelength channel detector temperature during a pericentre pass, Orbit 41, 22 January 2004.

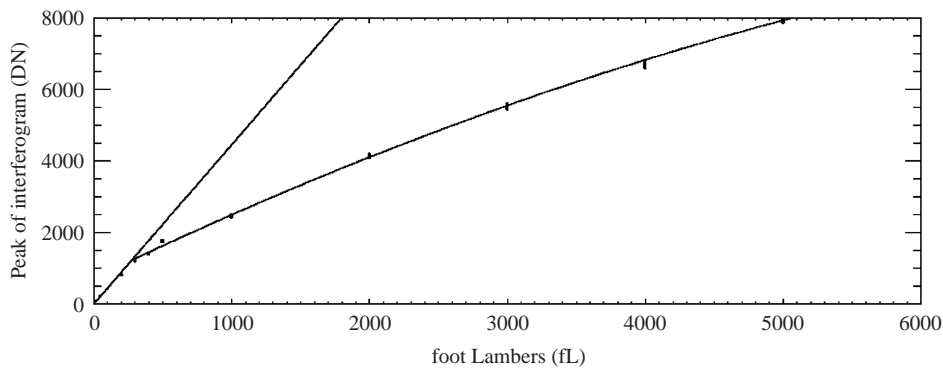


Fig. 2. Peak of symetrised interferogram versus source intensity.

The correction procedure is the following: from the value of y (and for all the y having absolute value larger than 1250) measured we compute x according to Eq. (1), then we compute a new value of y according to Eq. (2).

Forward and reverse motion of the pendulum have different Eqs. (1) and (2): for reverse motion, the values of the coefficients are:

$$a = -0.0000833814, \quad b = 1.86040, \quad c = 72.069, \\ a_1 = 4.45717, \quad b_1 = 0.0.$$

At Mars we have used, for reasons to be seen later, a gain factor of 8, which means that if there are points in the interferogram larger than 10,000 DN (= 1250 × 8) than the instrument is in nonlinear regime and these values must be corrected as described above.

2.3. Gain

The SW channel has 8 gain factors, namely 1, 2, 4, 8, 16, 32, 64, 128 experimentally verified. The linearity

behaviour has been tested for each of them. The nonlinearity starts always for the same source intensity (280 fL) unless the interferogram itself gets saturated because of the large amplification used.

When studying the behaviour of the calibrations, with the different gain factors we have identified a very important effect: the amplification increases the SNR; the reason for the increase of the SNR with increasing gain factors is in the fact that the noise of the SWC detector is lower than the noise of the AD converter; therefore the signal increases with the amplification, while the dominant noise does not. At gains above 8, the noise of the detector dominates over the noise of the digital electronics, and the SNR does not increase substantially. For this reason in space and at Mars we have first verified the behaviour, and then used almost always an amplification factor of 8.

2.4. The thermal part

The SW channel was planned to cover the spectral range from 8192 to 2000 cm^{-1} but it actually detects radiation below 2000 cm^{-1} down to 1700 cm^{-1} , recovering therefore part of the LW channel lost for the mechanical vibrations of the MEX spacecraft. From 1700 to $\sim 2900 \text{ cm}^{-1}$ the SWC detector behaves as a bolometer, i.e. it is sensitive to the temperature difference between the emitting source (T_s) and the

detector temperature; the amplitude of the measured signal is then depending on $\Delta T = |T_o - T_s|$.

The response of the instrument is different when observing sources above or below the detector temperature, because the interaction among them is different. For low signals (see Section 2.2 of this paper) the detector is linear but it has different coefficients for cold or hot sources, the responsivity being higher in the first case (see Fig. 3). This is very important because at Mars the source (the planet) can indeed be at temperatures lower or higher than the detector temperature (210–215 K). In Fig. 3 the measurements with the IKI Black Body (temperatures -100 , -60 , -30 , 0°C) and the IFSI BB (temperatures 30, 40, 50, 100°C) have been used.

2.5. Responsivity and NER

The result of the entire calibration activity in the Laboratory, is the Responsivity and NER for the PFS instrument. The responsivity, obtained by putting together the solar part obtained using the Integrating sphere, and the thermal part obtained using the measurements of the Black Body at different temperatures, is shown in Fig. 4. Atmospheric features still present are due to CO_2 and H_2O . This responsivity holds for spectra obtained from linearised interferograms, and transforms the computed Digital Numbers into radiance in CGS units $\text{ergs}/(\text{s sr cm}^2 \text{ cm}^{-1})$ simply by division.

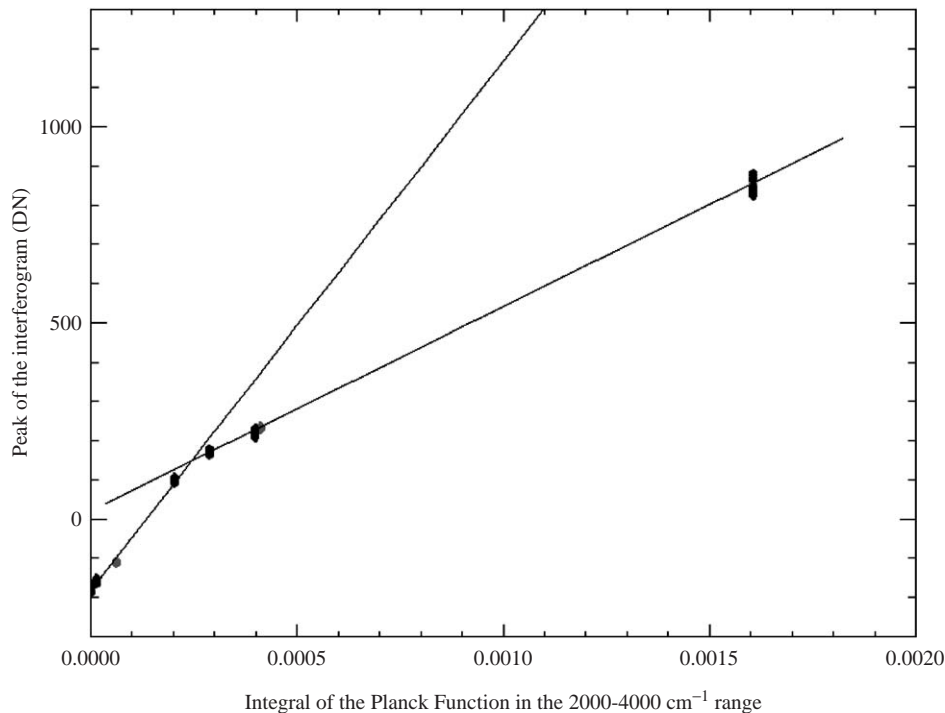


Fig. 3. Linearities of the SW channel in the thermal part. The peak of the interferogram is plotted versus the integral of the Planck function between 2000 and 4000 cm^{-1} for different temperatures (see text for details).

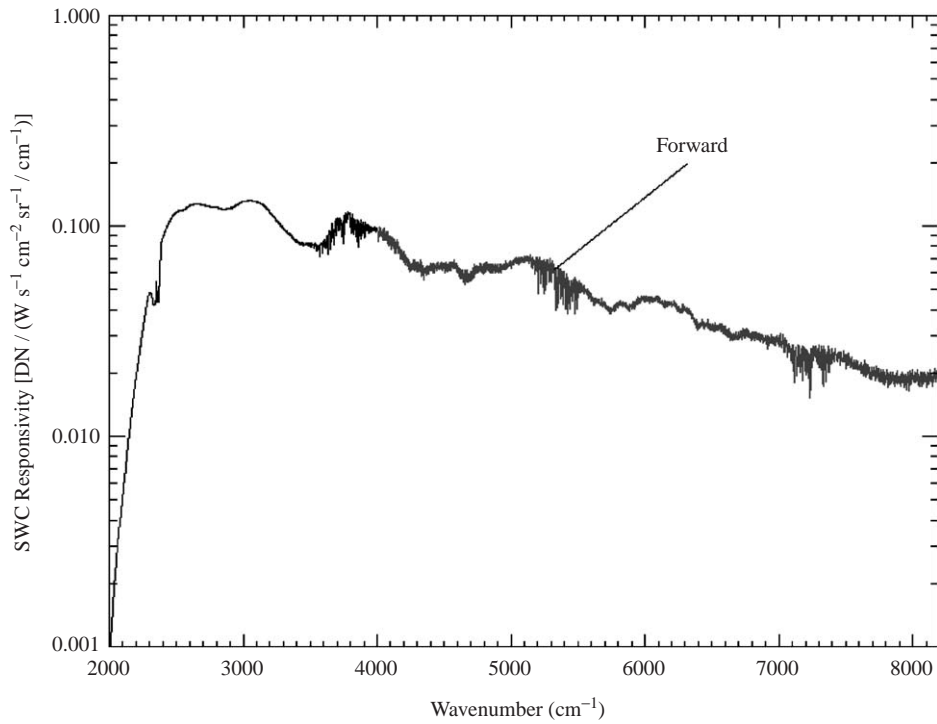


Fig. 4. Responsivity of the SW channel obtained in the Lab at room temperature and in air.

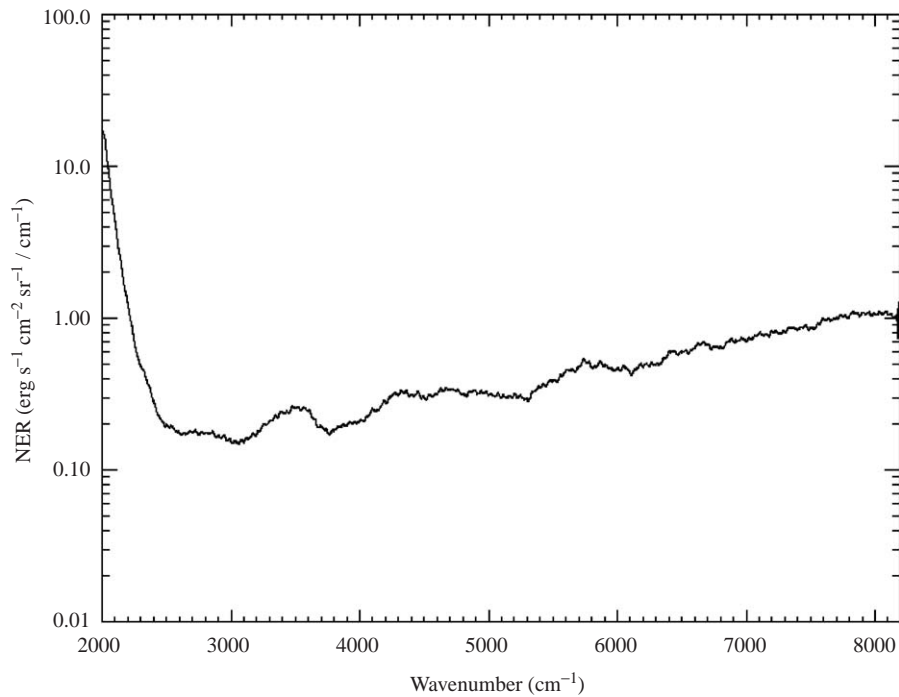


Fig. 5. Noise Equivalent Radiance for the SW channel at room temperature.

The NER is defined as the noise (sigma of the measurements) divided by the responsivity, and it is given in Fig. 5. The minimum of the NER is between 2500 and 3000 cm^{-1} in correspondence with the maximum of the Responsivity.

2.6. FOV

The FOV of the experiment was measured by moving a source on an $X - Y$ vertical plane, and by taking measurements in 30×30 different positions. The source

was at 1 m from the entrance of the interferometer, and in each position 10 measurements were taken. The entire system was computer controlled. The final result is shown in Fig. 6. The FWHM shows that the aperture of the SW channel is 1.7°, while the LW channel

aperture is 2.8°. The axis of the two channels are 1.8° apart.

2.7. Laser wavelength calibrations

The laser diodes used by PFS (see Paper I) are sensitive to temperature, i.e. the wavelength emitted, changes with temperature. This fact is very important because during a measurement session, if the thermal conditions are not stable, the step of our sampling will be changing from one measurement to another. The laser diode used, furthermore has the tendency to have ranges of temperatures in which the wavelength is constant, and ranges of temperatures in which the laser is not monochromatic and the double pendulum motion becomes perturbed, producing spiky interferograms. The two laser diodes used by PFS were calibrated in wavelength as function of temperature. Fig. 7 shows a step-like behaviour; this happens because a monochromatic line appears in a same PFS spectral channel (although deforming) until the laser diode temperature (wavelength) is such that the line is shifted to an adjacent spectral channel, producing a discontinuity in the behaviour. On Mars, both the laser diodes are under thermal control, but it needs some time to reach the set temperature.

The “minor” changes of the laser diodes Wavelength with the temperature inside a single step have been studied using a mercury lamp (in laboratory) and some very narrow and well known CO₂ lines (on Mars),

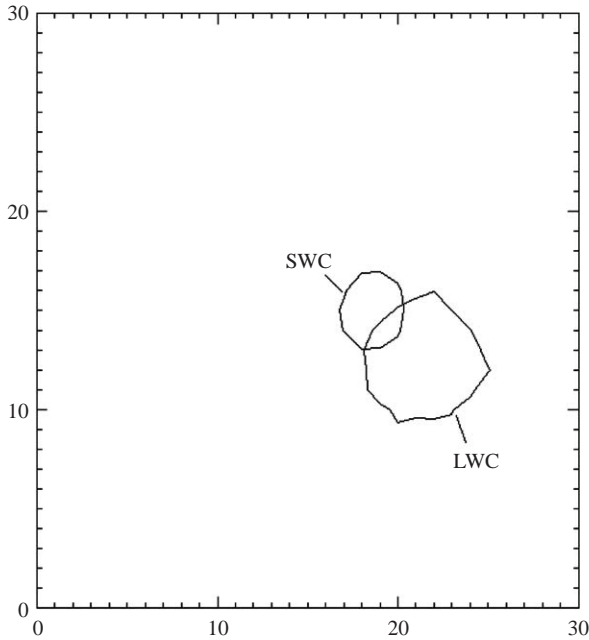


Fig. 6. FWHM for both channels LW and SW channels: the SW is 1.7° wide, while the LW is 2.8° wide. Note the displacement of the two channels of 1.8°. The two channels overlap only partially.

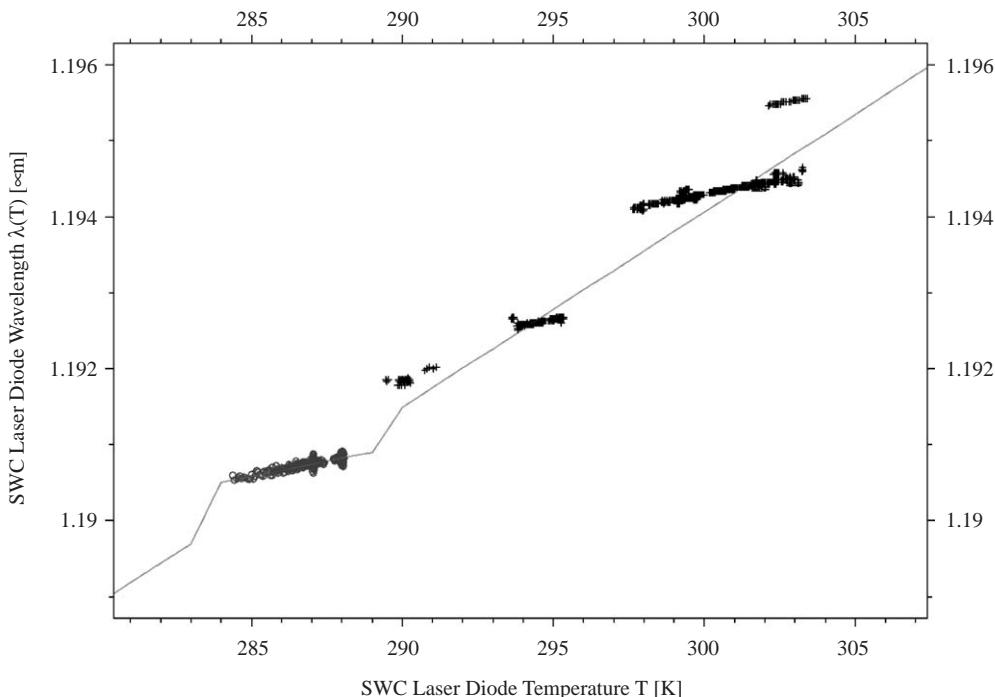


Fig. 7. SW channel laser diode behaviour with temperature.

together with the PFS monochromatic transfer function (see next section). On Mars, the laser diode temperatures vary approximately in the range 284–289 K for the SWC and inside these temperature ranges, the linear best fit is given by:

$$v \text{ (mm)} = 8.01631 \times 10^{-5} T + 1.16774.$$

For the whole temperatures range, an approximated linear fit can be used:

$$v \text{ (mm)} = 295.329 \times 10^{-6} T + 1.10584.$$

2.8. Monochromatic transfer function

The monochromatic transfer function of a spectrometer is a very important function that must be measured because it can introduce spurious features in the measurements. PFS transfer function was measured by looking at a monochromatic source (a mercury lamp) for a long time. The laser diode temperature, and therefore wavelength, changed with time (the source being fixed), therefore performing a relative shift between the source and the sampling point. The final result is a function of sinc type, while the instrument appears to have a spectral resolution (unapodised) of 1.3 cm^{-1} (see Fig. 8). The sinc function shows asymmetric overshooting and ringing, very important to keep in mind when studying thin single lines in the spectrum. These effects are much lower with apodisation. The apodised transfer function of PFS is shown in Fig. 9.

3. Detector cooling

All the results reported above have been obtained for the detector at room temperature, which also means that the thermal control and stabilisation of the detector, laser diode and instrument was not effective. We had, however, a number of tests with PFS in thermo-vacuum, and the detector cooled from room temperature 293–250 K. It has been found that cooling of the detector generates a linear-with-temperature and spectrally flat (outside the thermal range and below 6000 cm^{-1}) increasing of its responsivity. Above 6000 cm^{-1} , the responsivity still increases linearly, but with higher coefficients for higher wavenumbers (see Fig. 10). The much larger increase in the thermal part is *also* due to the fact that, in this spectral region, the signal depends on the difference between the source and the detector temperatures, as explained in Section 2.4: the lower is the detector temperature, the higher is this difference and thus the signal.

In the tests we were not able to achieve the temperature of 210–215 K planned for space, therefore we had to extrapolate the increase of the responsivity at that temperatures, to have an idea of the instrumental performance at the planned working conditions in space. Extrapolation at 212 K, which is the actual operating temperature at Mars, would give an increase of responsivity by a factor of ~ 5.5 as also shown in Fig. 11.

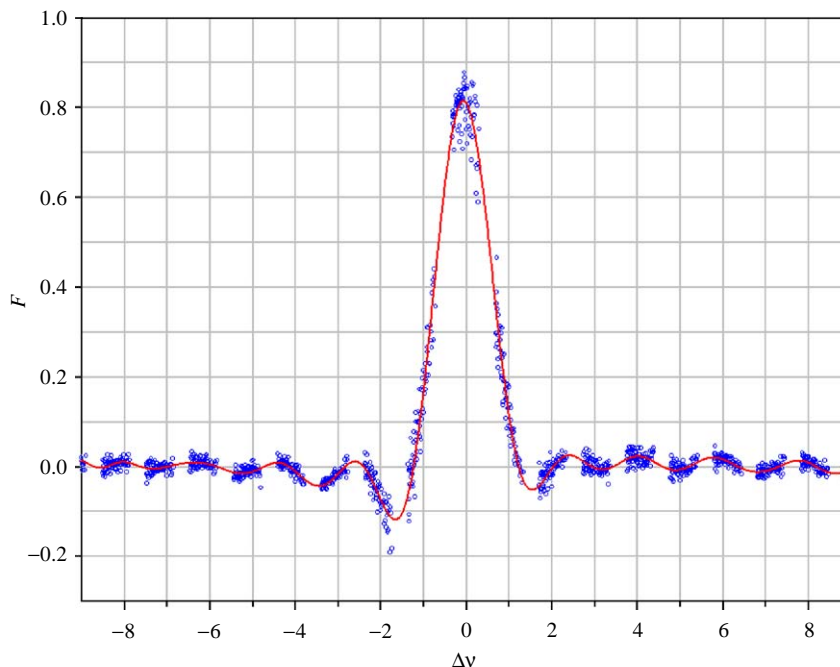


Fig. 8. Monochromatic transfer function of PFS measured with a Hg lamp. Horizontal units are cm^{-1} , vertical is line intensity.

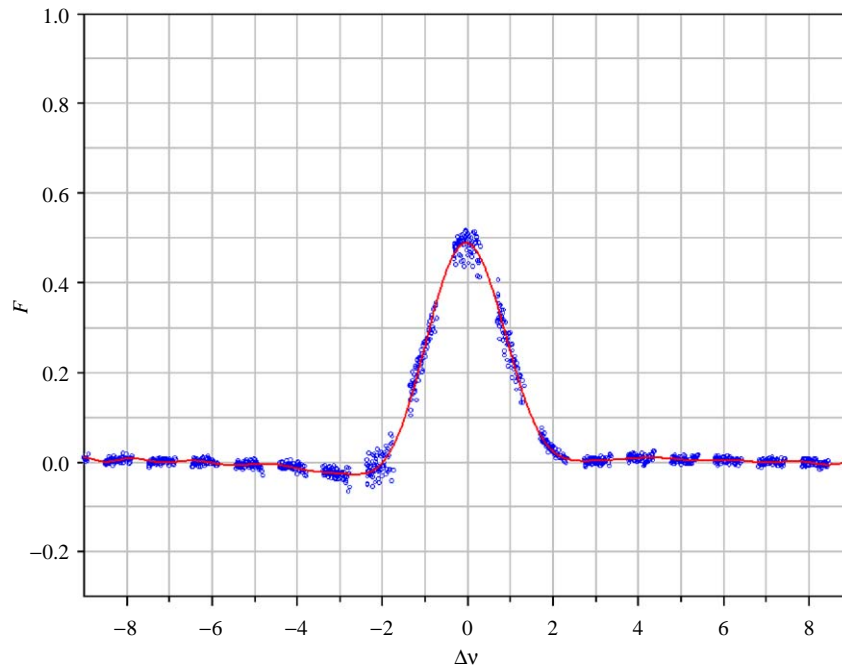


Fig. 9. The same as in Fig. 8, but apodised. Note that the spectral resolution becomes worse by a factor of 2.

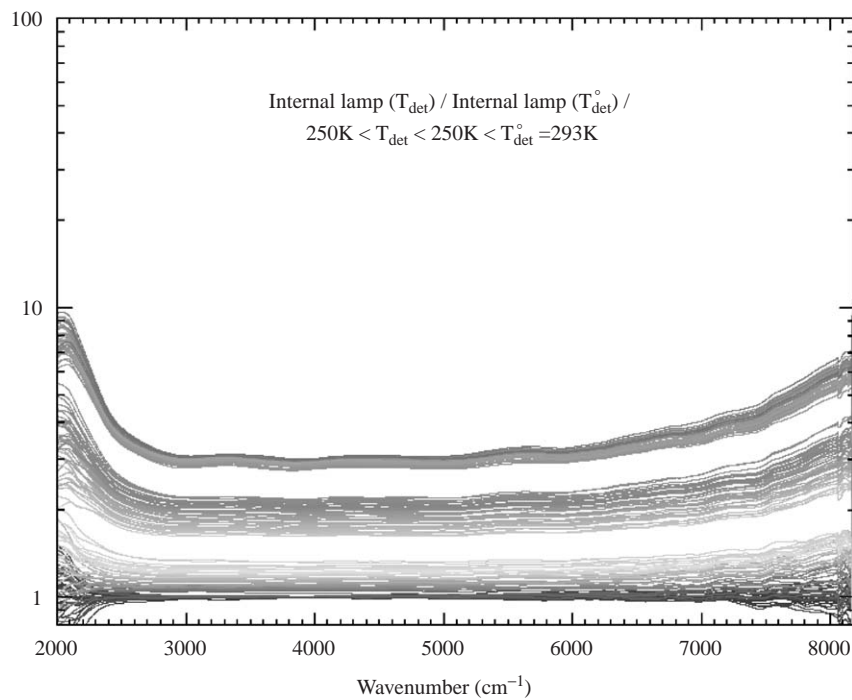


Fig. 10. Responsivity of the detector increase with its cooling.

If we compute the SNR in the two cases (i.e. with the detector temperature at 293 and 250 K), we find that the SNR is increased by roughly a factor 2, as the signal increases due to higher responsivity, while the noise does not, or increases by less amount.

4. SW channel in space (NEV activity)

In space, while certain things went as predicted, others went in an unpredictable way. In Fig. 1 it has already been shown the detector temperature stable and well

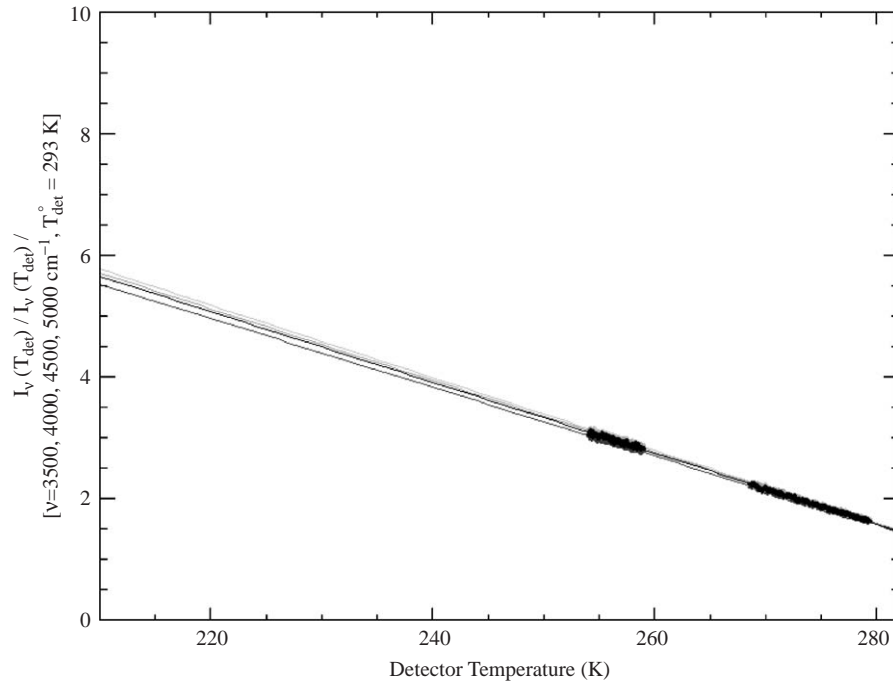


Fig. 11. Linear increasing of detector responsivity with decreasing detector temperature for different wavenumbers ($\nu = 3500, 4000, 4500$ and 5000 cm^{-1}). Values are normalised with respect to the room detector temperature (293 K).

controlled at 212 K during a pericentre pass; similarly, the SW Laser diode temperature is very well constant. This is a very important point for good motion of the pendulum and therefore interferograms without spikes.

In space we found two negative effects which we had to study, and resolve the problems that they were putting us, before proceeding:

- Mechanical vibrations of the spacecraft,
- Contamination on the pointing mirror.

4.1. Mechanical vibrations effects

The bandpass filter of the SW channel is $500\text{--}2000 \text{ Hz}$ when normal speed is used (speed called 2000 Hz). The mechanical vibrations discussed in Formisano et al. (this volume, Paper 1) and in Giuranna et al. (2005) are essentially at $10, 104, \text{ and } 570 \text{ Hz}$, and they modulate each other. Occasionally other frequencies appear, namely the $0.5 \times$ and the $2 \times$ of these fundamentals. These frequencies, the 590 and its modulations 650 and 545 Hz , appear directly in the SW channel range, and therefore are clearly seen. Fig. 12 shows the standard deviation for averages of 100 Deep Space spectra at different speeds of the double pendulum; they are constant at $\sim 0.2 \text{ DN}$ almost all over the range but show $5\text{--}10$ peaks in correspondence of the frequencies of the disturbances. The peaks resulting directly from the microvibrations at

the frequencies stated above, are seen at $2000\text{--}2800 \text{ cm}^{-1}$. The other peaks, much stronger, come into our frequency range indirectly by means of aliasing. This fact is demonstrated by studying the Deep Space spectra and their standard deviation as a function of the double pendulum speed. At speed 1500 Hz , the three direct disturbances are seen at $2900, 3450$ and 4200 cm^{-1} but, increasing the speed (2000 Hz), they move at 2150 and 2600 cm^{-1} (the first peak is outside the PFS range); at 2500 and 3000 Hz they are completely out of the official SW range (i.e. below 1750 cm^{-1}). Another set of three peaks of disturbances are, however, seen at $4900\text{--}5500 \text{ cm}^{-1}$ for speed 1500 Hz ; these peaks move in the opposite direction than the direct disturbances: when we go to speed 2000 Hz they are seen in the $5700\text{--}6300 \text{ cm}^{-1}$ range, then at speed 2500 Hz they are at $6200\text{--}6800 \text{ cm}^{-1}$, and at speed 3000 Hz they are at $6600\text{--}7000 \text{ cm}^{-1}$. This group, therefore, moves towards higher frequencies (apparently) and is essentially compressed, each peak becoming closer and closer to the others.

It should be noted that, averaging a certain number of spectra, in correspondence of these peaks of noise, the mean value of the spectrum is kept (see Fig. 13); therefore in the Near Earth Verification activity and testing, it was concluded that the experiment would also work well in flight if the conditions were disturbed, and that good Martian spectra would be achieved.

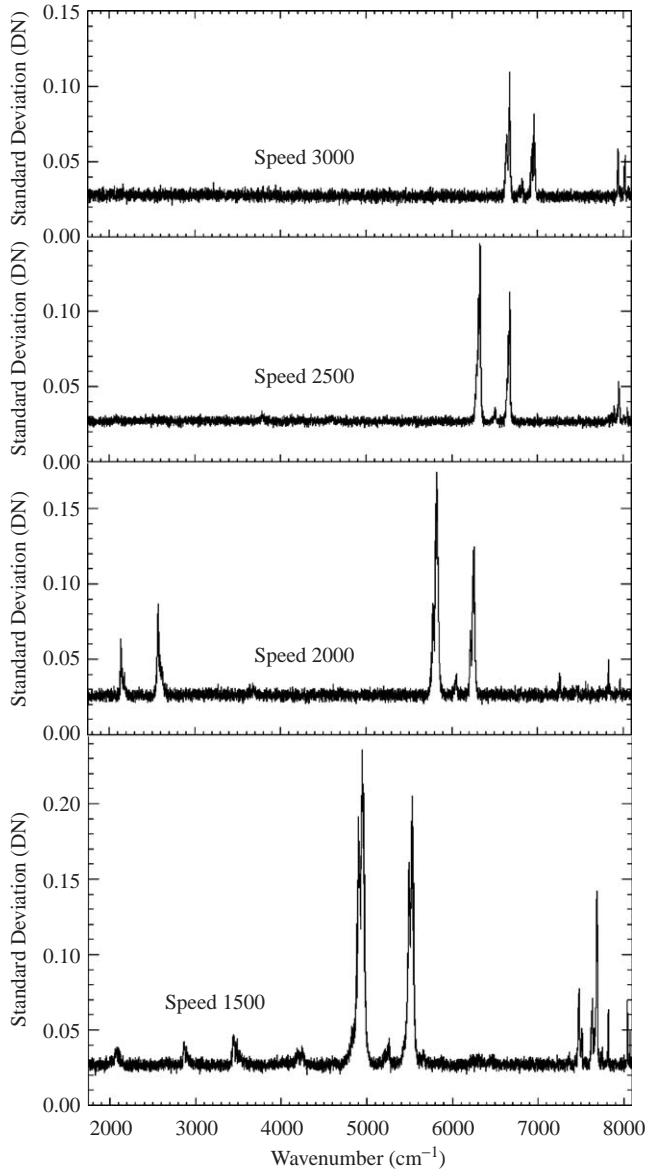


Fig. 12. Standard deviation for averages of 100 Deep Space measurements at different speeds of the double pendulum.

We can evaluate where a mechanical vibration line will be directly in the IR spectra in the following way:

$$N_{\text{dist}} = f_{\text{dist}} \frac{N_{\text{points}}}{f_{\text{samp}}}, \quad (3)$$

where f_{dist} is the frequency of the mechanical disturbance in Hertz, f_{samp} is the mean sampling frequency in Hertz, N_{point} is the number of points in the interferograms ($N_{\text{SW}} = 2^{14}$, $N_{\text{LW}} = 2^{12}$), N_{dist} is the position of the disturbance in the raw Fast Fourier Transform of the interferogram.

Mechanical vibrations, however, have another effect on PFS: they produce a cyclic misalignment of the optics (especially cubic corner mirrors). The result of such a misalignment is a cyclic reduction of the power towards

the detector. The resulting interferogram is modulated with the same frequencies of the disturbances. The consequence in the spectra of the interferogram is a couple of “satellites” around every IR emission line. The position of the disturbances for a certain IR line is:

$$N_{\text{dist}} = N_{\text{IRline}} \pm f_{\text{dist}} \frac{N_{\text{points}}}{f_{\text{samp}}}. \quad (4)$$

A consequence of this effect in SW channel is the modulation around the emission line of reference laser diode, that is exactly at Nyquist frequency of the spectra because the interferogram is acquired every $\lambda/2$ of the reference source. The reference laser beam uses the same optical path of analysed source, but it is out of the main beam: the only way to see the effect of laser in the main detector is to be found in internal reflections and light scattering.

The final consequence of laser diode line is that disturbances modulation generates a couple of “satellite” lines around the laser line, but the higher one is in aliasing and “is aliased” exactly over the lower frequency “satellite”.

$$N_{\text{dist}} = 8192 \pm f_{\text{dist}} \frac{N_{\text{points}}}{f_{\text{samp}}}. \quad (5)$$

To change the pendulum speed is equivalent to increase f_{samp} , therefore the distance from 8192 decreases for increasing speed.

At Mars the speed of 2500 Hz was used as compromise for the optimisation of SW and LW channels.

4.2. Contamination of the pointing mirror

It can be seen from Fig. 13 that, between 2800 and 3000 cm^{-1} , there is a spectral feature; this feature was absent in the laboratory measurements. We have been able to trace all the experiment activity until the Launch preparation activity in Baikonour. Still in Baikonour we had spectra of the Internal Calibration Lamp without this structure, so it must have been generated during the launching itself, or immediately after in space. The contamination is a hydrocarbon (or mixture) and the features are the stretch transitions of the CH_2 and CH_3 groups. The general shape of these bands has been verified to be essentially constant and can be corrected when generating the calibrated spectra (Fig. 14).

5. SW channel calibration at Mars

5.1. Spectral region $\nu \leq 3900 \text{ cm}^{-1}$

The SWC responsivity in the thermal region can be obtained in the same way as for the LW channel (Giuranna et al., 2005):

$$S(\nu) = R(\nu)I(\nu) - S_o(\nu), \quad (6)$$

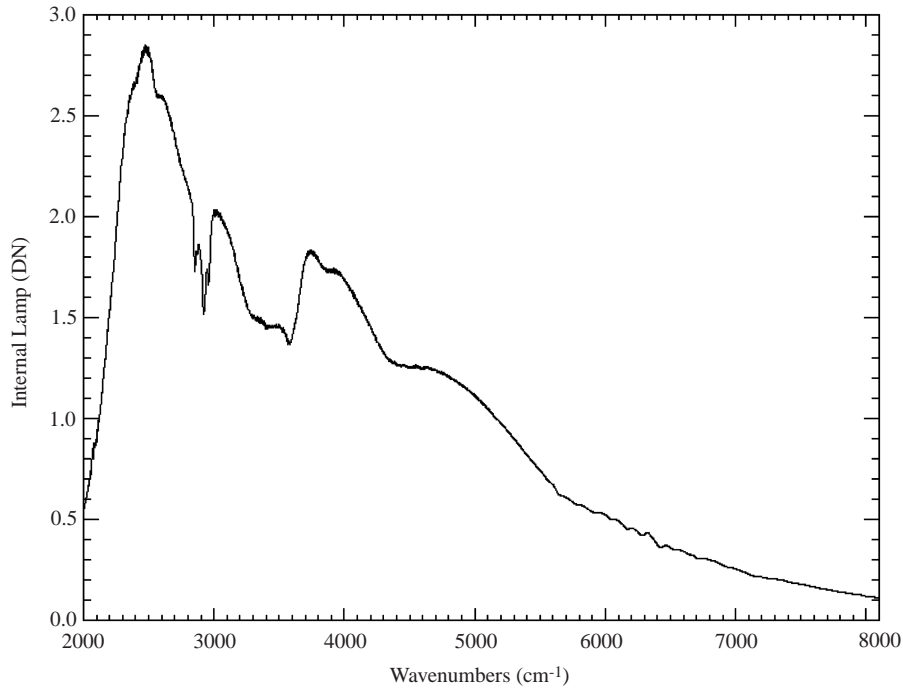


Fig. 13. Average of 200 Internal Lamp spectra. The effect of the mechanical vibration is almost absent.

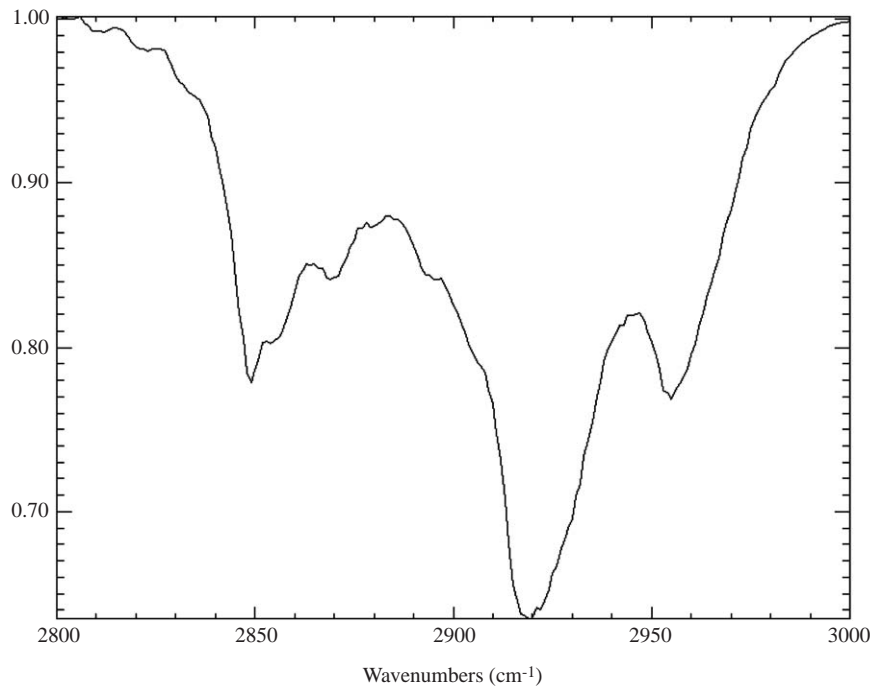


Fig. 14. Details of the contamination bands at 2800–000 cm^{-1} .

where $S(\nu)$ is the amplitude of a PFS SW channel spectrum when looking at a certain source, $I(\nu)$ is the radiance of the source, $S_o(\nu)$ is the emission of the instrument and $R(\nu)$ is the responsivity to be computed. We can use the Internal Blackbody as calibration source and the Deep Space measurements to estimate the

emission spectrum $S_o(\nu)$; this latter depends on the temperature of the interferometer which is not constant during a pericentre pass. Fortunately, we have Deep Space measurements just before and just after the pass, so we can interpolate the DS spectrum according to the interferometer temperature.

From the two in-flight calibration sessions, we can compute two responsivity curves by means of Eq. (6) that can be averaged; we know, however, that the SWC responsivity depends on the detector temperature (see Section 3): if it is not stable (see Fig. 1) we interpolate the responsivity according to the actual detector temperature during each Martian spectrum.

It must be said that, during the in-flight calibration sessions, we acquire only 10–20 spectra of the Internal Blackbody and Deep Space so that the responsivity curve computed by means of Eq. (6) is very noisy above $\sim 2600\text{ cm}^{-1}$. To solve this problem we used the calibration measurements acquired during the NEV activity (more than 200 spectra) and a comparison with the Infrared Space Observatory (ISO) SWS observations of Mars performed in July–August 1997 (see Formisano et al., 2005b).

5.2. Spectral region $\nu \geq 3900\text{ cm}^{-1}$

On the basis of Fig. 11 we predicted that in space, with the SW detector cooled, the Internal Calibration Lamp should have saturated, because of its high intensity, and because of the predicted increase of detector responsivity. Actually, we have seen that the spectrum of the internal lamp, with the detector cooled at 212 K, is only 1–2 times higher than the signal with the detector at room temperature. The reason for this can be found in a loss of optical alignment due, possibly, to the stress suffered by PFS during the launch phase.

The SWC responsivity on Mars in the solar spectral region is then given by:

$$R_{\text{Mars}}^{212\text{ K}}(\nu) = R_{\text{Lab}}^{293\text{ K}}(\nu)K(\nu)R_{2000}^{2500}(\nu), \tag{7}$$

where $R_{\text{Lab}}^{293\text{ K}}(\nu)$ is the responsivity obtained in laboratory, $K(\nu)$ is the actual increase of the SWC responsivity when passing from laboratory to space operating conditions and $V_{2000}^{2500}(\nu)$ is the function giving the spectral modifications introduced by the different speed used in space (2500 Hz), with respect the one used in laboratory (2000 Hz).

Joining the responsivities for the thermal and the solar range, one obtains the total SWC responsivity (Figs. 15 and 16).

5.3. Examples of calibrated Martian spectra

Samples of calibrated PFS data are shown here to illustrate the capabilities of the instrument and possible future science. An average spectrum in the $1750\text{--}4200\text{ cm}^{-1}$ wavenumber range is shown in Fig. 17. The spectrum shows a number of bands due to CO, CO₂ and water in the Martian atmosphere. We shall not go into the details of the measurement as this will be done in a following paper (Formisano et al., 2005b) while comparing PFS and ISO measurements. The only comment here is that the Planck function for $T = 275.5\text{ K}$ (the mean temperature of the averaged PFS spectra, as retrieved from the LWC spectra) fits very well the thermal part of the observations. Note that the

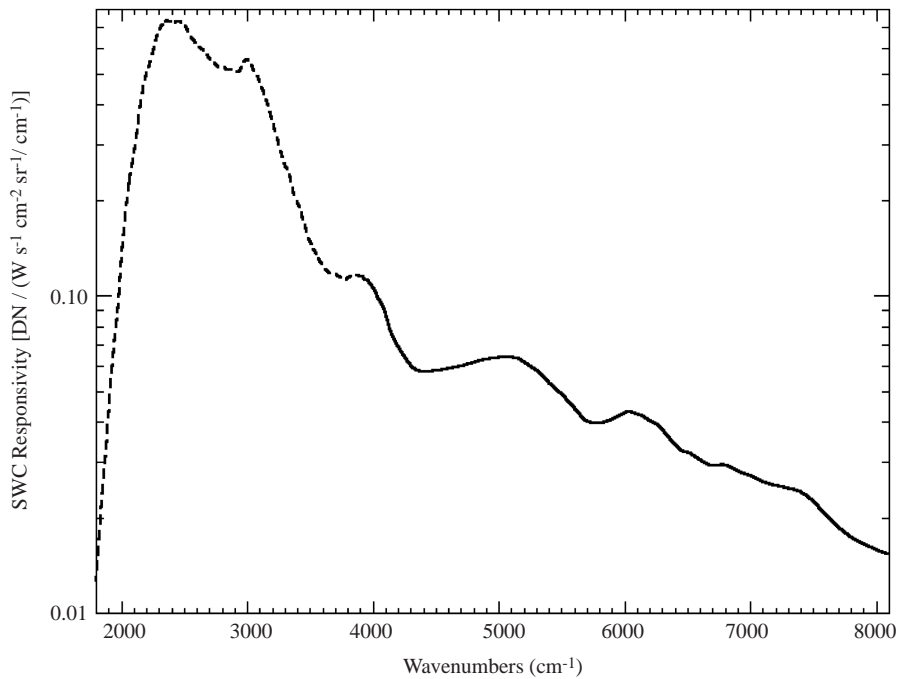


Fig. 15. Total Responsivity of the SW channel at space operating conditions, obtained joining the responsivities computed for the thermal (dashed) and the solar (line) range.

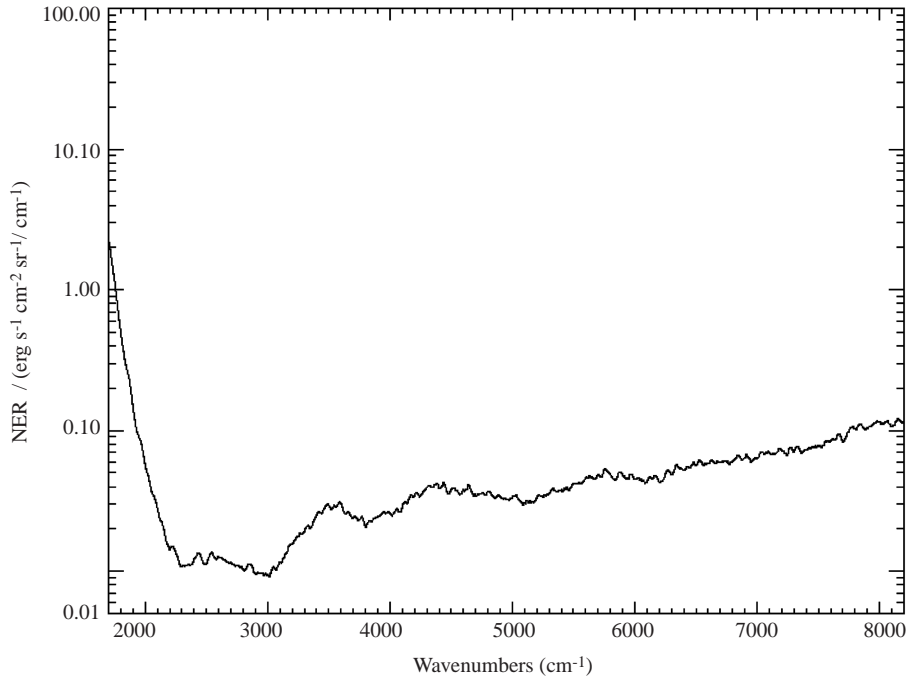


Fig. 16. The Noise Equivalent Radiance of the SW channel at space operating conditions. It is 10–20 times lower than the NER at room temperature (see Fig. 5)

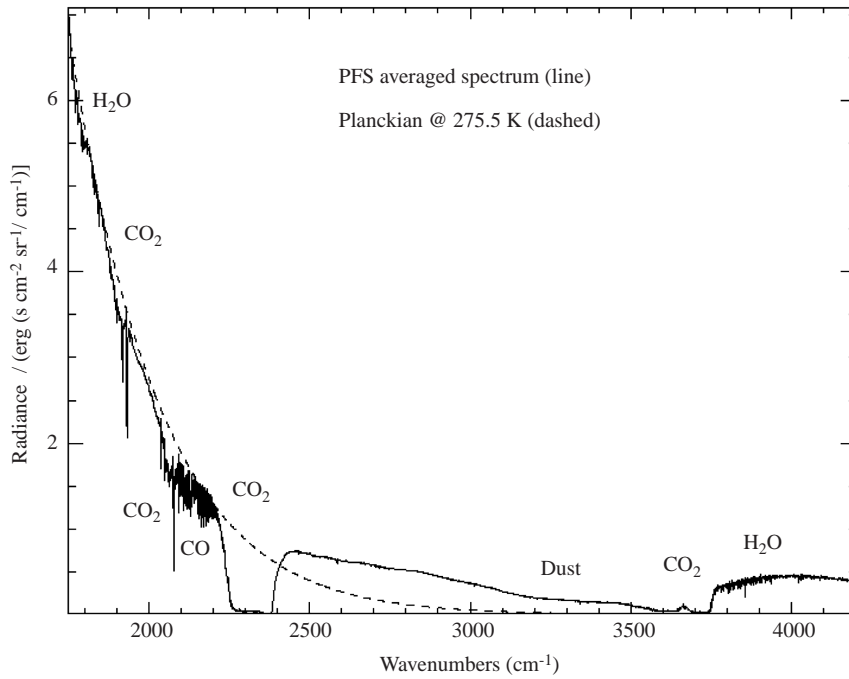


Fig. 17. A PFS calibrated average spectrum from 1750–4200 cm^{-1} . A Planck function for a BB temperature of 275.5 K fitting the thermal part is shown (dashed line).

spectrum shown was an average over 1680 measurements, selected so to have high radiance (namely within $\pm 45^\circ$ in latitude around the subsolar point, at 14:00 local time).

We show now four portions of the previous calibrated spectrum, compared with a synthetic spectrum computed for the Martian atmosphere: these are possible main topics of research for future studies.

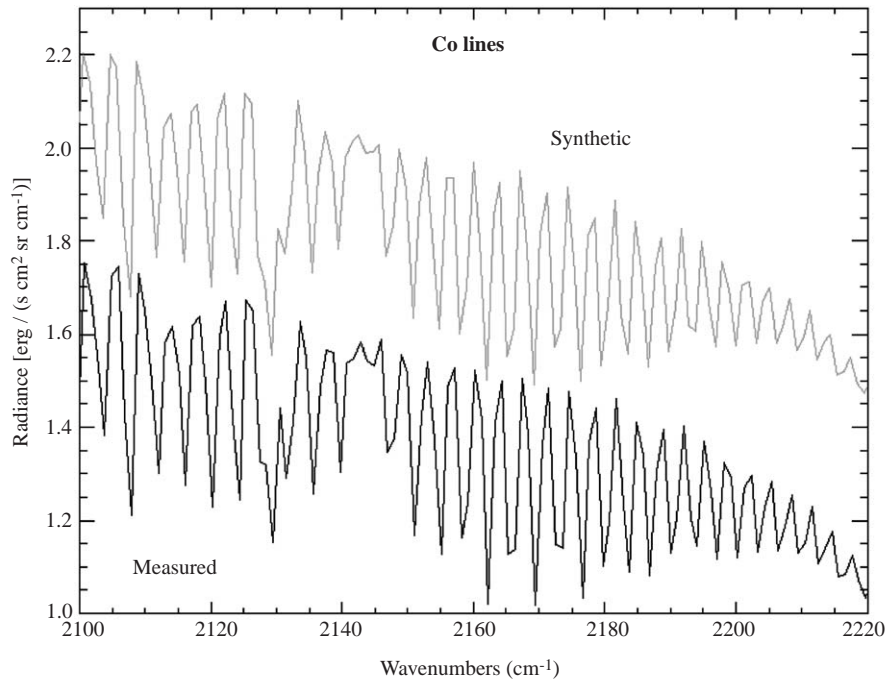


Fig. 18. The CO absorption lines in the 4.7 μm range. The synthetic spectrum is computed for 825 ppm of CO and is shown shifted by 0.45 CGS units for comparison.

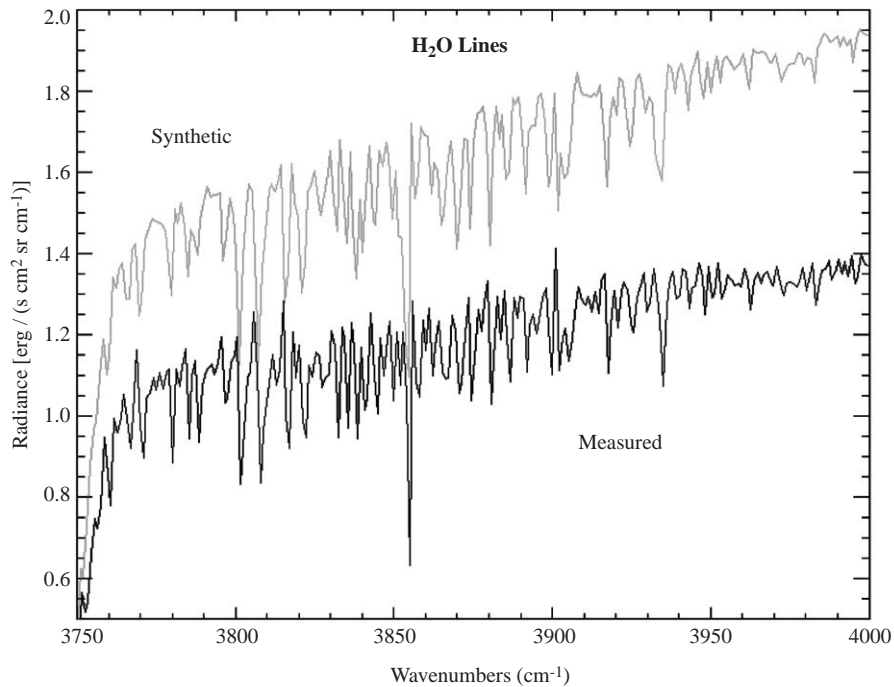


Fig. 19. Water lines in the 2.7 μm range. The synthetic spectrum is computed for 300 ppm of H_2O and is shown shifted by 0.5 CGS units for a better comparison.

CO lines are shown in Fig. 18 together with a synthetic spectrum computed with 825 ppm of CO.

Water lines are shown in Figs. 19 and 21 together with a synthetic spectrum computed with an H_2O mixing ratio of 300 ppm.

In Fig. 20 we show a portion of the solar spectrum which is being used for PFS analysis (see Fiorenza and Formisano, 2005) together with the measured spectrum of PFS: almost all the measured absorption lines appear to be due to the Fraunhofer solar lines; a solar spectrum

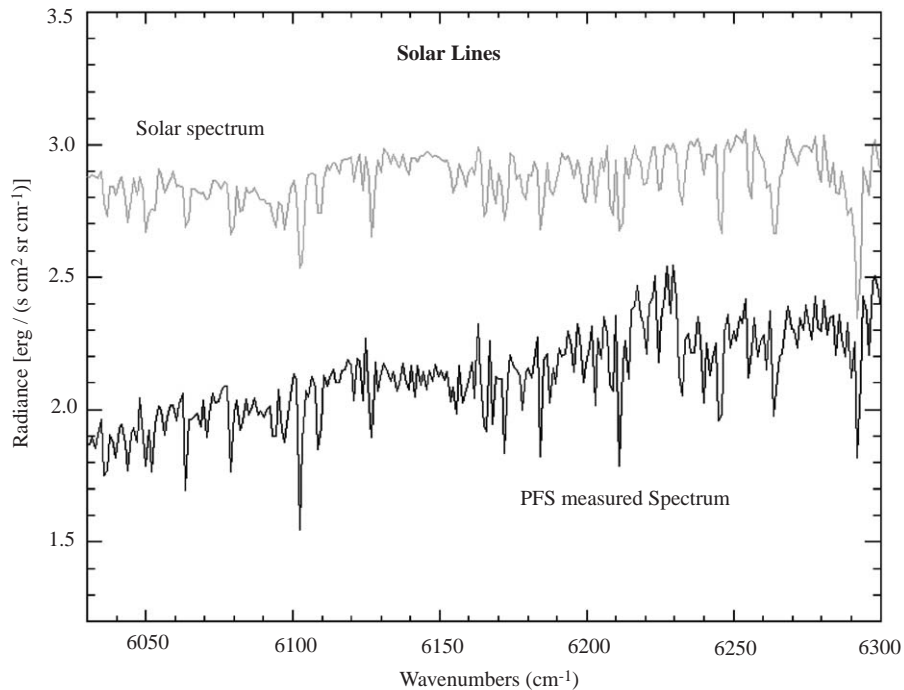


Fig. 20. Mars spectrum as measured by PFS (bottom) together with a pure solar spectrum (top).

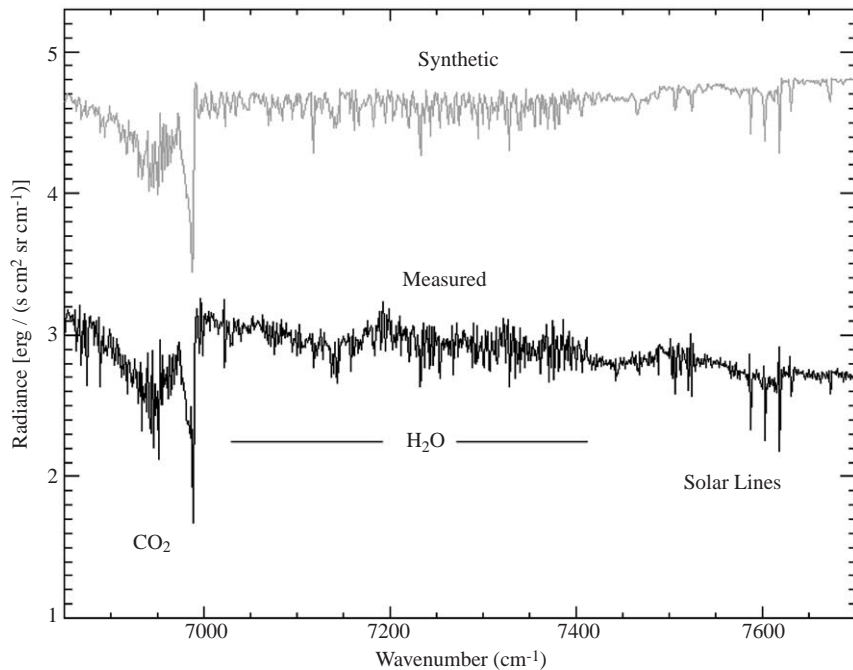


Fig. 21. PFS measured and synthetic (shifted by 1.5 CGS units) spectrum in the 6850–7700 cm^{-1} range showing a nonsaturated CO_2 band, a few solar and many water lines.

in this wavenumber range had never been measured from space with this spectral resolution (Fig. 21). We measure the solar spectrum as reflected by Mars, but still these measurements may be important to verify the presence of computed lines in the solar spectrum.

In Fig. 22 we finally show three single spectra in the 2000–2400 cm^{-1} range; in this spectral region the Signal-to-Noise ratio for a single spectrum is higher than 100 in a hot region (i.e. high thermal emission). The bottom line of Fig. 22 is the spectrum observed

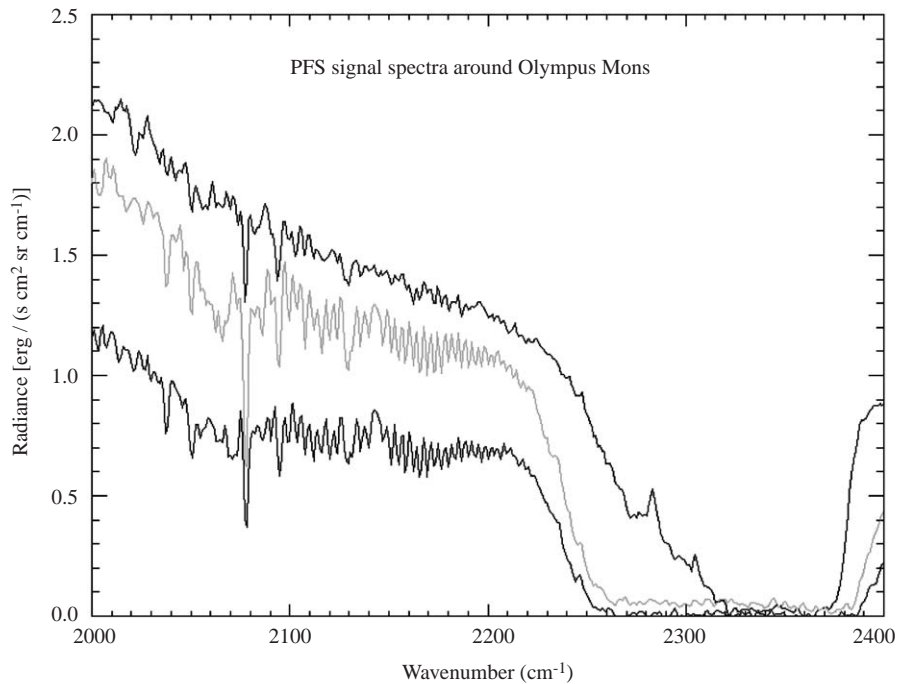


Fig. 22. Single spectra measured by PFS south of the Volcano (gray), on top the caldera (top) and north of it in the plain (bottom). Only a short part of the SW channel spectrum is shown, to evidence the decrease of the CO₂ and CO on top of the mountain.

north of the Olympus Mons, the gray one is south of the volcano while the top one is measured inside the caldera. The large decrease of radiance in the interval 2240–2390 cm⁻¹ is due to the 4.3 μm CO₂ band. Normally this is a saturated band (whose radiance level in the centre of the band may indicate nonLTE; see Formisano et al., 2005b) but the reduced CO₂ amount on top the volcano allows features at 2280 cm⁻¹, normally annihilated in the bottom of the saturated band, to become now visible. Also, CO decreases on top the volcano as can be clearly seen from the top curve of Fig. 22, which although being with a higher continuum, shows weaker CO lines.

We are able to model the CO, and get the actual mixing ratio along the track of the orbit, but this is not the task of this paper.

Acknowledgements

The PFS experiment has been built at the *Istituto di Fisica dello Spazio Interplanetario (IFSI)* of *Istituto Nazionale di Astrofisica (INAF)*, and has been founded by the Italian Space Agency (ASI) in the context of the Italian participation to the ESA's Mars Express Mission.

Appendix A

Owing to phase errors all original interferograms have an asymmetric form. Asymmetry of the central part of

the interferogram has been corrected by means of the specially developed algorithm based on the method of phase correction (Forman and Howard, 1966). We name the corrected interferogram as “symetrised”.

However, the method of the phase correction allows phase errors correction about accuracy up to 80°, i.e. about accuracy up to the sign of the spectrum of continuum. We used the additional information about the sign of the spectrum of the continuum, accessible a priori. We have information on the temperature of the PFS detector, the temperature on the “black body”, the temperature of “cold” space, and also taking into account that the temperature of the surface of Mars in observable areas is less than temperature of the detector, we can unambiguously assign the sign to the corrected continuum.

References

- Fiorenza, C., Formisano, V., 2005. A solar spectrum for PFS data analysis. *Planet. Space Sci.*, this volume, doi:10.1016/j.pss.2004.12.008.
- Forman, M., Howard, W., 1966. Correction of asymmetric interferograms obtained in the fourier spectroscopy. *J. Opt. Soc. Am.* 56, 59–63.
- Formisano, V. and the PFS Team, 2005a. The Planetary Fourier Spectrometer (P.F.S.) onboard the European Mars Express Mission. *Planet. Space Sci.*, this volume, doi:10.1016/j.pss.2004.12.006.
- Formisano, V., et al., 2005b. A Martian PFS average spectrum: comparison with ISO SWS. *Planet. Space Sci.*, this volume, doi:10.1016/j.pss.2005.03.009.

Giuranna, M., Formisano, V., Biondi, D., Ekonomov, A., Fonti, S., Grassi, D., Hirsch, H., Khatuntsev, I., Ignatiev, N., Michalska, M., Mattana, A., Maturilli, A., Mencarelli, E., Nespoli, F., Orfei, R., Orleanski, P., Piccioni, G., Rataj, M., Saggin, B., Zasova, L., 2005. Calibration of the PFS LW channel. *Planet Space Sci.*, this volume, doi:10.1016/j.pss.2005.02.007.

Further reading

Formisano, V., Mattana, A., Biondi, D., Mencarelli, E., Nespoli, F., Rossi, M., Maturilli, A., Giuranna, M., Grassi, D., Piccioni, G., Saggin, B., Fonti, S., Hirsch, H., 2002. PFS instrument calibration report, vol. I, IFSI Internal Note.

Formisano, V., Giuranna, M., Grassi, D., Maturilli, A., Piccioni, G., Saggin, B., Fonti, S., Hirsch, H., Zasova, L., Ignatiev, N., Mattana,

A., Biondi, D., Mencarelli, E., Nespoli, F., Rossi, M., 2003a. PFS instrument calibration report, vol. II, IFSI Internal Note.

Formisano, V., Mattana, A., Giuranna, M., Biondi, D., Nespoli, F., Mencarelli, E., Rossi, M., Maturilli, A., Piccioni, G., Saggin, B., Michalska, M., Grygorczuk, J., 2003b. PFS instrument calibration report, vol. III—PFS space calibration, IFSI Internal Note.

Hanel, R.A., et al., 1970. Infrared spectroscopy experiment for mariner Mars 1971. *Icarus* 12, 48–62.

Hanel, R., et al., 1972. Mariner 9 Michelson interferometer. *Appl. Opt.* 11 (11), 2625–2634.

Hanel, R.A., et al., 1992. *Exploration of the Solar System by Infrared Remote Sensing*. Cambridge University Press, Cambridge First published.

Hirsch, H., 1997. Optical design and performance of the planetary fourier spectrometer. *Microchim. Acta* 14 (Suppl.), 571–574.